International Journal of Pharmaceutics xxx (xxxx) 124183

Contents lists available at ScienceDirect

International Journal of Pharmaceutics

journal homepage: www.elsevier.com/locate/ijpharm

RGD-tagging of *star*-shaped PLA-PEG micellar nanoassemblies enhances doxorubicin efficacy against osteosarcoma

Roberto Oliva [a], Serena Maria Torcasio [a, b], Olivier Coulembier [b], Anna Piperno [a], Antonino Mazzaglia [c], Silvia Scalese [d], Arianna Rossi [a, e], Giada Bassi [e, f], Silvia Panseri [e], Monica Montesi [e], Angela Scala [a, *]

[a] *Department of Chemical, Biological, Pharmaceutical and Environmental Sciences, University of Messina, V.le F. Stagno d'Alcontres 31, 98166 Messina, Italy*
[b] *Center of Innovation and Research in Materials and Polymers (CIRMAP), Laboratory of Polymeric and Composite Materials, University of Mons, Place du Parc 23, 7000 Mons, Belgium*
[c] *CNR-ISMN, National Council of Research, Institute for the Study of Nanostructured Materials, URT of Messina c/o Department of Chemical, Biological, Pharmaceutical and Environmental Sciences, University of Messina, V.le, F. Stagno d'Alcontres, 31, 98166 Messina, Italy*
[d] *CNR-IMM, Consiglio Nazionale delle Ricerche – Istituto per la Microelettronica e Microsistemi, Ottava Strada n.5, 95121 Catania, Italy*
[e] *CNR-ISSMC, Institute of Science, Technology and Sustainability for Ceramics, Via Granarolo 64, 48018 Faenza, RA, Italy*
[f] *Department of Neuroscience, Imaging and Clinical Science, University of Studies "G. D'Annunzio", 66100 Chieti, CH, Italy*

ARTICLE INFO

Keywords:
Drug delivery
Nanoparticles
Block copolymers
Dimerization
Targeting
Peptide

ABSTRACT

We developed cyclic RGD-tagged polymeric micellar nanoassemblies for sustained delivery of Doxorubicin (Dox) endowed with significant cytotoxic effect against MG63, SAOS-2, and U2-OS osteosarcoma cells without compromising the viability of healthy osteoblasts (hFOBs). Targeted polymeric micellar nanoassemblies (RGD-NanoStar@Dox) enabled Dox to reach the nucleus of MG63, SAOS-2, and U2-OS cells causing the same cytotoxic effect as free Dox, unlike untargeted micellar nanoassemblies (NanoStar@Dox) which failed to reach the nucleus and resulted ineffective, demonstrating the crucial role of cyclic RGD peptide in driving cellular uptake and accumulation mechanisms in osteosarcoma cells. Micellar nanoassemblies were obtained by nanoformulation of three-armed *star* PLA-PEG copolymers properly synthetized with and without decoration with the cyclic-RGDyK peptide (Arg-Gly-Asp-D-Tyr-Lys). The optimal RGD-NanoStar@Dox nanoformulation obtained by nanoprecipitation method (8% drug loading; 35 % encapsulation efficiency) provided a prolonged and sustained drug release with a rate significantly lower than that of the free drug under the same experimental conditions. Moreover, the nanosystem preserved Dox from the natural degradation occurring under physiological conditions (*i.e.,* dimerization and consequent precipitation) serving as a slow-release *"drug reservoir"* ensuring an extended biological activity over the time.

1. Introduction

Tumors localized in the bone, such as osteosarcoma (OS), remain incurable fatal diseases owing to the fast clearance or non-specific binding profile of currently available therapeutics. In addition, the solid composition and the large surface area of bones prevent the drugs to reach the target site and represent the major drawback in treating bone malignancy (Panez-Toro et al., 2023). Standard OS chemotherapy based on cytotoxic drugs (*i.e.,* doxorubicin, cisplatin, methotrexate) can improve the overall 5-year survival rate up to 70 % but their severe side effects affect the life quality (Gianferante et al., 2017). Therefore, OS treatment remains to be challenging due to the low rate of both new approved candidate drugs and innovative therapeutic strategies; no prominent advancements have been made in the past 20 years from any scientific areas including nanomedicine. Several drug nanocarriers have been designed for OS treatment (Wang et al., 2020) but most of them are still confined to the experimental arena and further studies are needed for OS-targeted delivery strategies and controlled drug release before clinical application.

Polymeric micelles with *core–shell* architecture have gained increasing interest as excellent carriers for drug and gene delivery (Kuperkar et al., 2022; Agrahari and Agrahari, 2018; Piperno et al., 2021). Specifically, unimolecular micelles formed by the *self-assembly* of *star* copolymers exhibit outstanding properties such as high drug loading capacity

* Corresponding author.
E-mail address: ascala@unime.it (A. Scala).

https://doi.org/10.1016/j.ijpharm.2024.124183
Received 12 February 2024; Received in revised form 27 April 2024; Accepted 28 April 2024
0378-5173/

and excellent *in vivo* stability owing to their covalently reinforced *core–shell* globular structure that prevents disassembly upon dilution. Moreover, *star* polymers can be properly decorated at their terminal groups with suitable ligands (*e.g.,* peptides, antibodies, aptamers, folic acid, etc) for active targeting (Ren et al., 2016). Among the plethora of targeting ligands developed to date, RGD (Arg-Gly-Asp) is a well-studied tumor-homing peptide that specifically binds integrins overexpressed on cancer cells and blood vessels during cancer angiogenesis. The extracellular binding domains of integrins are readily accessible by RGD-tagged drug delivery systems (DDS) promoting their internalization by receptor-mediated endocytosis followed by intracellular trafficking to endosomes and/or lysosomes and drug release into the cytoplasm (Battistini et al., 2021; Zhang et al., 2023). Several papers reported that cyclic RGD peptides covalently anchored to the nanoparticle (NPs) surface promoted higher binding affinity and selectivity to specific integrins (*e.g.,* a_vb_3 and a_vb_5 are expressed in some OS cell lines) respect to linear RGD due to the restriction of their conformational freedom (Rios De La Rosa et al., 2020; Li et al., 2021).

To the best of our knowledge, no earlier studies proposed the use of cyclic RGD-decorated polymeric NPs for targeted therapy of OS, although it is well known that RGD can improve the effective delivery of anticancer drugs including doxorubicin (Dox) (Sun et al., 2017). With this in mind, in the framework of our research program for designing novel polymer-based nanotherapeutics (Oliva et al., 2023; Mineo et al., 2020; Liénard et al., 2020; Scala et al., 2018; Fazio et al., 2015), we herein develop cyclic RGD-tagged *star*-shaped PLA-PEG micellar nanoassemblies loaded with Dox (RGD-NanoStar@Dox) and we compare the biological outcomes of targeted and untargeted micellar nanoassemblies (RGD-NanoStar@Dox and NanoStar@Dox, respectively, Fig. 1) against MG63, SAOS-2, and U2-OS osteosarcoma cells.

In the last few years, several classes of nanomaterials have been exploited as Dox carriers for OS treatment, including liposomes, exosomes, polymeric NPs, hydroxyapatite and metal NPs (NPs) (Parchami et al., 2023; Wei et al., 2022; Yang et al., 2020; Liu et al., 2023; Lupusoru et al., 2020). In most of them, Dox molecules were overloaded to achieve the desired therapeutic efficacy because they often lack the right nuclear localization and release the drug into the cytoplasm, so that only approximately 1 % of Dox could reach the nucleus and keep active (Song et al., 2021). Since Dox overloading could be responsible for short- and long-term side effects (*e.g.,* cardiotoxicity, nausea, myelosuppression, gastrointestinal disorders, etc.), the development of drug nanocarriers for effective nuclear delivery of Dox is gaining substantial interest as it is expected to increase safety and to enhance efficacy.

Our nanocarrier is based on amphiphilic *star* PLA-PEG copolymer synthetized by a proper combination of ring-opening polymerization (ROP) and copper-catalyzed azide-alkyne cycloaddition (CuAAC) reactions (Torcasio et al., 2022). The tumor-targeting ligand cyclic-RGDyK peptide was covalently linked to the end-groups to be eventually exposed on nanocarrier surface. Our recent work (Torcasio et al., 2022) investigated the ability of *star* PLA-PEG-RGD to encapsulate the antitumoral drug Docetaxel focusing on the effects on U87 Human Glioblastoma and MDA-MB 468 Human Breast Adenocarcinoma cell lines, as models of two most common primary and metastatic tumors. A stronger ability of the drug-loaded PLA-PEG-RGD nanocarrier to reduce tumor propagation and invasiveness was observed compared to the free drug in both cell lines attesting for an enhanced effect on metastatization respect to free Docetaxel. These biological findings, together with the absence of toxicity on healthy cells, prompted us to further investigate our fascinating polymeric nanoshuttle focusing on Dox for OS treatment.

Herein, the biological profiles of two nanosystems, with and without cyclic RGD-tagging (*i.e.,* RGD-NanoStar@Dox and NanoStar@Dox, respectively), were studied and compared in terms of cellular uptake and cytotoxicity, focusing on the MG63, SAOS-2, and U2-OS cell lines. Human fetal osteoblast cells (hFOBs) were used to test the effect of nanocarriers on healthy cells.

Dox was encapsulated using different nanoformulation methods (*i.e.,* nanoprecipitation and dialysis) and two polymer-to-drug mass ratios were explored (*i.e.,* 10:1 and 10:3). Physicochemical properties (*i.e,*

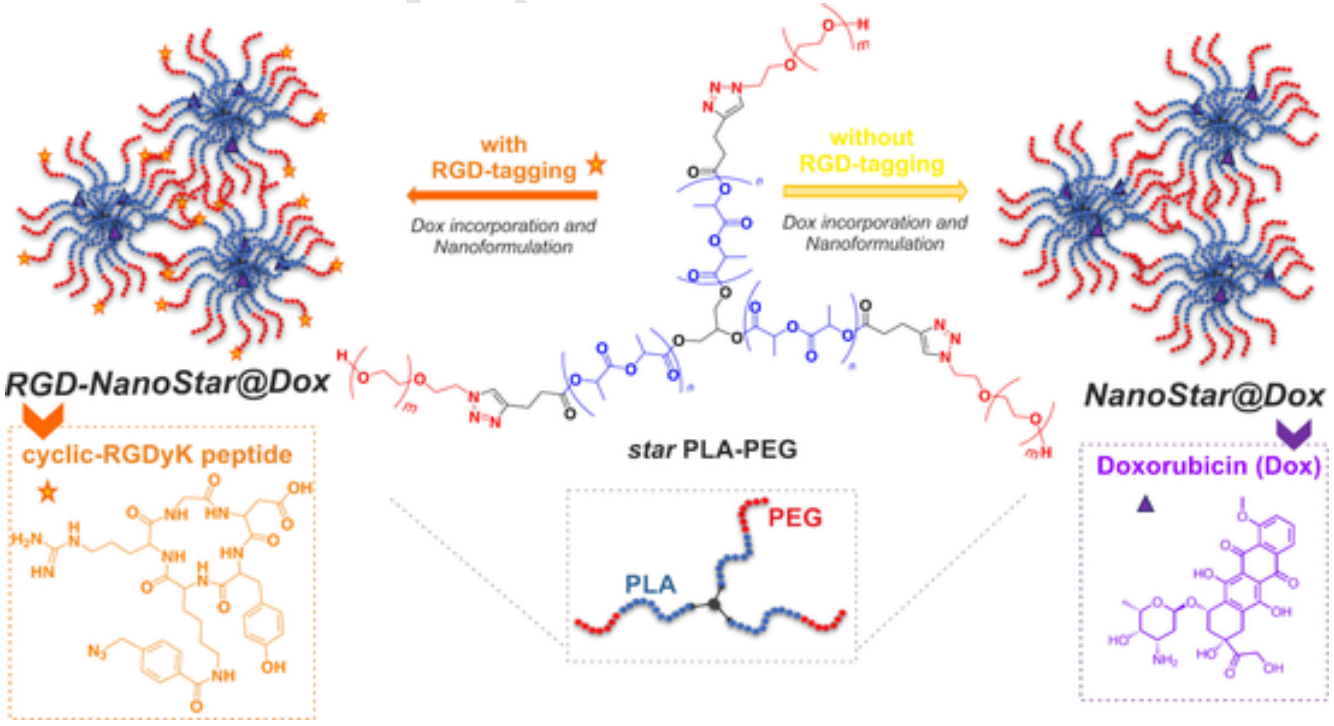

Fig. 1. Chemical structure and sketched view of three-armed *star* PLA-PEG copolymer used to prepare RGD-NanoStar@Dox (left) and NanoStar@Dox (right), with and without cyclic RGD-tagging, respectively. The insets reported the chemical structure of cyclic-RGDyK peptide (Arg-Gly-Asp-D-Tyr-Lys) and Doxorubicin (Dox).

particle size, size distribution, zeta potential), drug loading, encapsulation efficiency, drug release profile and morphology were investigated. The biological outcomes of our study confirmed the great potential of cyclic RGD-based strategies for targeted anticancer therapy. Moreover, our release data pointed out that the proposed nanosystem protect the drug from dimerization under physiologically relevant conditions and, consequently, could assure an extended biological activity over the time.

2. Material and methods

2.1. Materials

Azido cyclic RGDyK was purchased from Scintomics. Doxorubicin hydrochloride (Dox HCl), triethylamine (TEA), methanol, tetrahydrofuran (THF), dimethyl sulfoxide (DMSO), ultrapure water, PBS (Phosphate Buffered Saline) (0.01 M, 1X, pH 7.4), and other reagents were purchased from Merck (Italy).

2.2. Instrumentation

A Labconco FreeZone lyophilizer was used for freeze-drying. ^{1}H NMR spectra were recorded on a Varian 500 MHz spectrometer at room temperature (25 °C). UV/Vis spectra were recorded on a Jasco V-730 spectrophotometer using 1 and 0.5 cm path length quartz cells. Hydrodynamic diameter (D_H) and size were determined in ultrapure water by photon correlation spectroscopy (PCS) using a Zetasizer Nano ZS (Malvern Instruments, Malvern, U.K.) at 25 °C. The measurements were performed at 173° angle to the incident beam at 25 ± 1 °C for each aqueous dispersion. The deconvolution of the correlation curve to an intensity size distribution was obtained using a non-negative least-squares algorithm. The zeta potential values (ζ) were measured using a Zetasizer Nano ZS Malvern Instrument equipped with a He − Ne laser at a power P = 4.0 mW and λ = 633 nm. The results are reported as the mean of three separate measurements in three different batches ± standard deviation (SD).

2.3. Synthesis

The synthesis of *star* PLA-PEG copolymer and *star* PLA-PEG-RGD was carried out according to previous studies (Torcasio et al., 2022).

2.4. Preparation of NanoStar@Dox

2.4.1. Nanoprecipitation

Dox HCl (3 mg) was solubilized in THF (1 mL) and 1 equiv. of TEA (0.7 μL) was added for deprotonation. The mixture was stirred in the dark for 2 h, followed by centrifugation at 4500 rpm for 5 min. This solution was combined with a solution of *star* PLA-PEG copolymer (30 mg) dissolved in 2 mL of THF (final polymer concentration:10 mg/mL; 10:1 polymer-to-drug mass ratio). The organic solution was added dropwise to 15 mL of stirring ultrapure water (1:5 THF: water ratio). After 24 h, THF was evaporated under reduced pressure and the suspension was centrifuged twice at 13.000 rpm for 15 min. The residue was freeze-dried to obtain NanoStar@Dox as a red powder. Similarly, empty NanoStar was prepared using the same method without adding the drug and used as a blank.

2.4.2. Dialysis

Dox HCl (9 mg) was solubilized in 1 mL of a 1:1 mixture of methanol and DMSO, followed by the addition of 2.2 mL of TEA and *star* PLA-PEG copolymer (30 mg; 10:3 polymer-to-drug mass ratio). The solution was stirred in the dark for 1 h and then added dropwise to 20 mL of stirring ultrapure water. After 4 h, the suspension was transferred into a dialysis bag (cut-off 3.5–5 KDa) and dialyzed against 800 mL of ultrapure water for 24 h. As the time elapsed, DMSO was replaced with water and the micellar nanoassemblies were gently formed inside the bag. The dialyzed suspension was freeze-dried to obtain NanoStar@Dox as red powder.

2.5. Preparation of RGD-NanoStar@Dox

Dox HCl (9 mg) was dissolved in THF (1.5 mL), TEA (2.2 μL) was added, and the solution was stirred in the dark for 15 min for Dox deprotonation. A blended mixture of *star* PLA-PEG (27 mg) and *star* PLA-PEG-RGD (3 mg) dissolved in THF (1.5 mL) was added (10:3 polymer-to-drug mass ratio). The resultant organic solution was stirred for 5 min and then added dropwise to 30 mL of stirring ultrapure water. After 4 h, THF was evaporated under reduced pressure and the suspension was centrifuged twice at 13.000 rpm for 15 min. The residue was freeze-dried to obtain RGD-NanoStar@Dox as a red powder. Similarly, empty RGD-NanoStar was prepared using the same method without adding the drug and used as a blank.

2.6. Drug loading

Drug content and loading efficiency were determined using UV–Vis spectroscopy. A weighed amount of lyophilized NanoStar@Dox or RGD-NanoStar@Dox was solubilized in DMSO, UV–Vis spectra were recorded, and the amount of encapsulated drug was calculated at a wavelength of 482 nm. A calibration curve for Dox in DMSO was constructed in the concentration range 9.5–95 μg/mL. Based on the molar extinction coefficient (ε ≅ 11450 M^{-1} cm^{-1}) and the absorbance, drug loading (DL) and encapsulation efficiency (EE) were calculated using the following equations:

$$DL(\%) = (Drug\,weight\,in\,the\,NPs / Weight\,of\,the\,drug - loaded\,NPs) \times 10$$

$$EE(\%) = (Drug\,weight\,in\,the\,NPs / Weight\,of\,drug\,used\,in\,the\,formulation) \times$$

2.7. Size and zeta potential

Dynamic light scanning (DLS) and ζ-potential measurements were performed on the lyophilized samples reconstituted in ultrapure water (1 mg/mL), sonicated in an ultrasonic bath for 15 min and diluted to a final concentration of 0.3 mg/mL.

2.8. SEM analysis

Morphological and structural characterization of nanoassemblies was performed by scanning electron microscopy (SEM), using a field emission scanning electron microscope (Supra35 FE-SEM by Zeiss, Oberkochen, Germany). RGD-NanoStar and RGD-NanoStar@Dox dispersed in ultrapure water (0.03 mg/mL) were deposited by drop-casting on a silicon substrate and, after drying, were analyzed using low energy (3 keV) electron beam, in order to prevent any damaging of the nanoassemblies.

2.9. Drug release

RGD-NanoStar@Dox (2 mg containing 160 μg Dox, based on the DL value) or NanoStar@Dox (3.2 mg containing 160 μg Dox, based on the DL value) were dispersed in 1 mL of PBS (0.01 M, 1X, pH 7.4), sonicated for 15 min, and transferred into a dialysis tube (Spectra Por® Prewetted RC Tubing MWCO 3.5–5 kDa). Dialysis was performed against 5 mL of PBS at 37 °C. At fixed time points (45 min, 1 h 30 min, 3 h 30 min, 5 h, 6 h, 8 h, 24 h, 48 h, and 72 h), 1 mL of the release medium was withdrawn, replaced with an equal volume of fresh buffer, and analyzed by UV–Vis spectroscopy to quantify the released Dox (λ_{max}

480 nm). All experiments were performed in duplicates. A calibration curve for Dox in PBS was previously constructed in the concentration range 3.3–149 μg/mL ($\varepsilon \cong 9752\ M^{-1}\ cm^{-1}$). Free Dox in PBS was dialyzed under similar experimental conditions at the same concentration (160 μg/ml).

2.10. Dox stability study

Solutions of Dox HCl in PBS at three different concentrations (*i.e.,* 300 μM, namely 160 μg/mL, the same concentration used for the release experiment; 60 μM and 6 μM) were maintained at 37 °C and the UV–Vis absorption was analyzed at λ_{max} 480 nm at fixed times (45 min, 1 h 30 min, 3 h 30 min, 5 h, 6 h, 8 h, 24 h, 48 h, 72 h). Dox degradation was indirectly quantified by measuring the amount of residual Dox in the supernatant.

2.11. Evaluation of CMC

The CMC of *star* PLA-PEG and *star* PLA-PEG-RGD was determined using the pyrene fluorescence spectroscopy method (Torcasio et al., 2022). Briefly, a stock pyrene solution in acetone (6×10^{-6} M) was prepared and added to a series of vials, followed by acetone evaporation. A polymer solution (concentration range $1 \times 10^{-3} - 0.1$ mg/mL) was added to the vials and, after equilibration at room temperature overnight, the emission fluorescence intensities at 338 and 333 nm were registered. The intensity ratio of I_{338}/I_{333} *vs.* the log of the copolymer concentration was used to determine the CMC.

2.12. Cell culture

All human cell lines were purchased from the American Type Culture Collection (ATCC). Human Osteosarcoma cell line MG63 (ATCC® CRL-1427™) was cultured in DMEM/F-12 GlutaMAX (Gibco) supplemented with 10 % fetal bovine serum (FBS) (Gibco) and 1 % penicillin/streptomycin mixture (Pen/Strep) (Gibco). Human Osteosarcoma SAOS-2 and U2-OS were cultured in McCoy's 5 Modified Medium (Gibco), supplemented with 15 % and 10 % FBS, respectively, and 1 % Pen/Strep. Human Fetal Osteoblastic (hFOBs) cell line was cultured in DMEM/F12 no phenol red with L-glutamine supplemented with 10 % FBS and 0.3 mg/mL Geneticin (Gibco). Cells were incubated at 37 °C, 5 % CO_2 under controlled humidity conditions. Cells were detached from the flask by trypsinization and centrifuged. The cell number and viability were assessed using the Trypan Blue Dye Exclusion Test. All cell handling procedures were performed under sterile conditions in a laminar flow hood.

2.13. In vitro study of Dox-loaded/-unloaded NanoStar and RGD-NanoStar

The biological activity of NanoStar and RGD-NanoStar loaded and unloaded with Dox was tested *in vitro* on three osteosarcoma cell lines and hFOBs as a model of healthy cells, using Dox HCl (European Pharmacopoeia) as a positive control and cells only as a negative control. Briefly, NanoStar@Dox and NanoStar were tested *in vitro* at 5.4 μg/mL drug concentration and 105 μg/mL NanoStar concentration. RGD-NanoStar@Dox was tested *in vitro* at 2.7 μg/mL, 5.4 μg/mL and 10.8 μg/mL drug concentration. Unloaded RGD-NanoStar was tested in culture media at the same concentration used to test RGD-NanoStar@Dox (*i.e.,* 31, 62 and 124 μg/mL of polymeric micelles for 2.7 μg/mL, 5.4 μg/mL and 10.8 μg/mL of Dox, respectively). The samples were reconstituted in MilliQ water at a concentration of 1 mg/mL and they were re-suspended in tip sonicator for 5 min at 20 % amplitude (A) before final dilution in culture media. All cell lines were seeded at a density of 5000 cells/well in 96 well-plates.

2.14. Cellular uptake

The cellular uptake of both NanoStar and RGD-NanoStar loaded with Dox at 5.4 μg/mL concentration was analyzed in all cell lines after 72 h of culture with respect to free Dox. Specifically, the cells were fixed in 4 % buffered paraformaldehyde (PFA), permeabilized in PBS 1X with 0.1 % (v/v) Triton X-100, and DAPI (600 nM, Invitrogen) counterstaining was performed to highlight cell nuclei, following the manufacturer's instructions. Images of the TRITC and DAPI filters were acquired using an inverted Ti-E fluorescence microscope (Nikon) and merged to observe the nuclear internalization of Dox in the cells. One experiment was performed and a biological duplicate was performed for each condition.

2.15. MTT assay

The viability of all cell lines grown in the presence of the samples was evaluated after 72 h of culture by the MTT assay, following the manufacturer's instructions. Briefly, the MTT reagent [3-(4,5-dimethylthiazol-2-yl)-2,5-diphenyltetrazolium bromide] (5 mg/mL) was dissolved in PBS 1X and the cells were incubated with MTT solution for 2 h at 37 °C, 5 % CO_2 and controlled humidity conditions. The medium was replaced by incubation for 15 min in DMSO with slight stirring and the absorbance was read at 570 nm using a Multiskan FC Microplate Photometer (Thermo Scientific). Absorbance values were directly proportional to the number of metabolically active cells. One experiment was performed and a biological triplicate was performed for each condition.

2.16. Cell morphology evaluation

The morphology of all the cell lines was analyzed after 72 h of culture with unloaded RGD-NanoStar at the highest concentration tested (124 μg/mL). Briefly, cells were fixed in 4 % PFA and permeabilized in PBS 1X with 0.1 % (v/v) Triton X-100. F-actin filaments were highlighted using a green-fluorescent Alexa Fluor 488® phalloidin probe (Life Technologies) for 20 min incubation, following the manufacturer's instructions. DAPI counterstaining was performed for cell nuclei identification following the manufacturer's instructions. Images were acquired using an Inverted Ti-E fluorescence microscope. One experiment was performed and a biological duplicate was performed for each condition.

2.17. Statistical analysis

Statistical analyses were performed using the GraphPad Prism Software (8.0.1. version). The results of the MTT assay are reported in the graphs as the mean percentage of cell viability with respect to cells only ± standard error of the mean and were analyzed by One-way and Two-way analysis of variance (One-way and Two-Way ANOVA) and Tukey's multiple comparisons test (* $p \leq 0.05$, ** $p \leq 0.01$, *** $p \leq 0.001$, **** $p \leq 0.0001$).

3. Results and discussion

3.1. Chemistry

The chemical strategy for the preparation of three-armed *star* PLA-PEG copolymer consisted of a multi-step synthesis (Torcasio et al., 2022) involving a ring-opening polymerization (ROP) of L-lactide, using glycerol as an initiator, to achieve the hydrophobic three-armed *star* PLA core ($Mn^{1H\ NMR} = 14.000$ g/mol; $Mn^{SEC,app} = 21.019$ g/mol),

followed by a series of esterification reactions with pentynoic anhydride and copper-catalyzed azide-alkyne cycloaddition (CuAAC) reactions for the subsequent conjugation of both the hydrophilic moiety

(*i.e.,* PEG, Mw 2000 g/mol for each arm) and the targeting ligand (*i.e.,* cyclic RGD peptide) to the PLA core (Scheme 1). Specifically, the decoration with RGD was achieved by reacting the three-armed alkynyl-terminated *star* PLA-PEG copolymer with two equivalents of azido cyclic-RGDyK peptide by CuAAC with a coupling efficiency of approximately 50 % (~1.5 degree of substitution). A stable triazole-based linkage between polymer scaffold and RGD peptide was created by copper-mediated cycloaddition as confirmed by ^{1}H NMR spectroscopy (Fig. S1) and SEC analysis (Torcasio et al., 2022). This decoration did not affect the molar mass of the copolymer as the peptide contribution was negligible (RGD MW 892 g/mol) with respect to the high molecular weight of the whole polymer ($Mn^{SEC,app}$ = 34.203 g/mol). However, the conjugation of RGD at the PEG chain to be eventually exposed on the nanocarrier surface strongly influenced the biological profile of RGD-NanoStar@Dox driving them to the cell nucleus, whereas the undecorated NanoStar@Dox failed to reach the nucleus, resulting ineffective (see Biological section).

The designed chemical pathway, characterized by high conversion efficiency and mild reaction conditions, allowed a fine control over the polymeric architecture in terms of chemical composition, number of arms, polymerization degree, molecular weight, and hydrophilic-to-hydrophobic ratio; the latter is crucial to guarantee the *self-assembly* of the amphiphile in water exerting a significant effect on polymer micellization in aqueous solution. In fact, literature data suggested that particle size and micellar aggregation behavior of PLA-PEG copolymers are strongly dependent on their composition (Govender et al., 2000; Riley et al., 2001). Specifically, a strong dependence on the length of the hydrophobic PLA block was observed when the *core*-forming blocks dominate the micellar structure, pointing out that the hydrodynamic radius

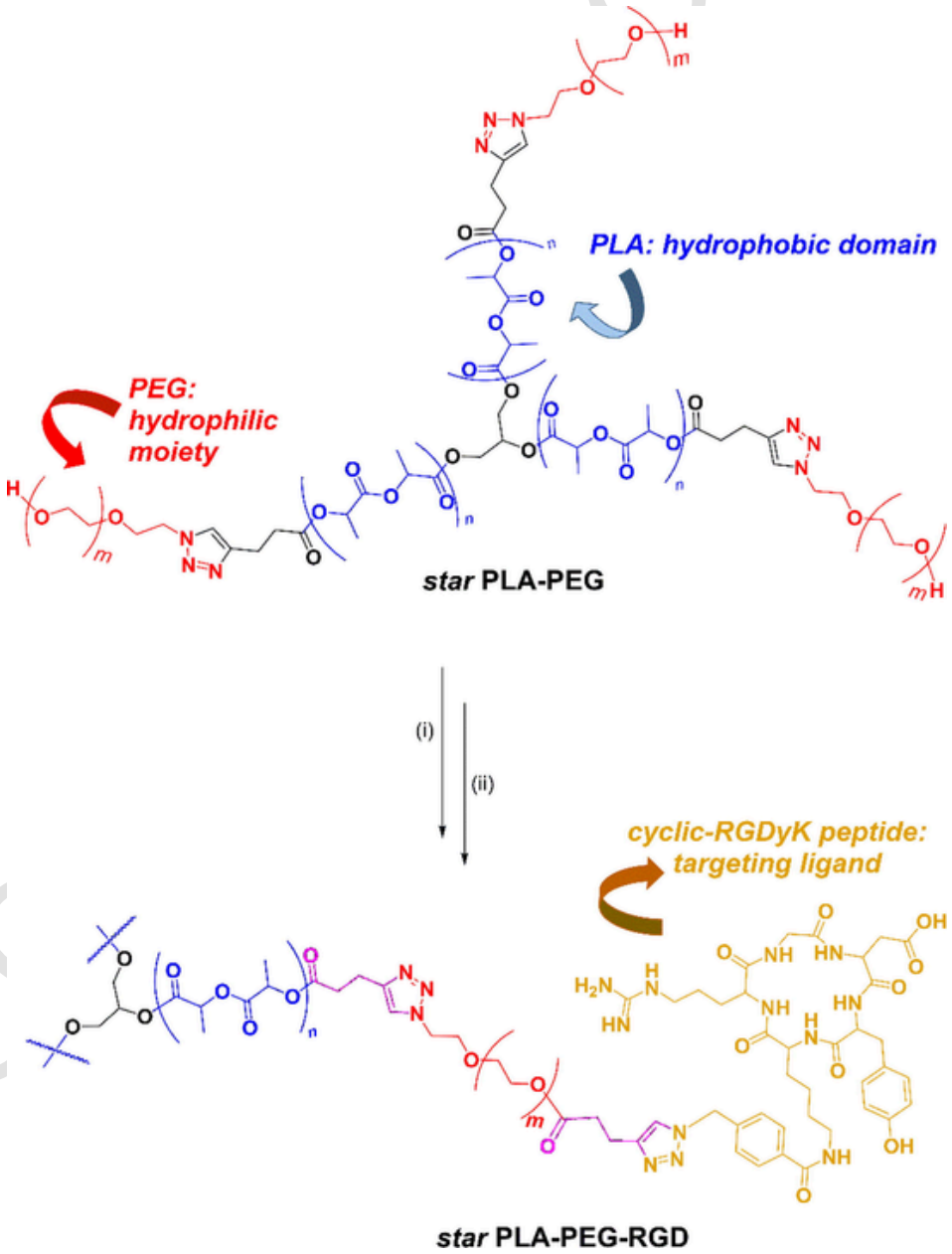

Scheme 1. Chemical pathway for the synthesis of three-armed *star* PLA-PEG-RGD starting from *star* PLA-PEG copolymer. Reagents and conditions: *(i: esterification of terminal OH groups)* pentynoic anhydride, DMAP, dry DCM, r.t., 12 h; *(ii: CuAAC for decoration of PLA-PEG with RGD)* azido cyclic-RGDyK peptide, CuBr, PMDETA, dry THF, r.t., 16 h.

of the particle is effectively equal to the radius of the *core*, being dependent on the number of monomeric units in the *core*-forming blocks.

The favorable Critical Micelle Concentration (CMC) value of both *star* PLA-PEG and *star* PLA-PEG-RGD (*i.e.,* 0.01 mg/mL) attested that micelles constituted by *star* polymers could be formed below CMC values typically expected for linear amphiphilic copolymer. Consequently, they are generally stable upon high dilutions because of the covalently reinforced *core–shell* architecture (Lotocki and Kakkar, 2020) providing a long circulation time in the bloodstream, which is an important factor for drug delivery.

To fully investigate both polymers (*i.e.,* untargeted *star* PLA-PEG and targeted *star* PLA-PEG-RGD) from a physicochemical and biological point of view and to compare their potential as DDS, we first studied the undecorated *star* PLA-PEG whose outcomes allowed to optimize the subsequent investigation on RGD-tagged *star* PLA-PEG.

3.2. NanoStar formulation and characterization

The nanoformulation of *star* PLA-PEG was carried out by nanoprecipitation and dialysis to explore different techniques for NanoStar preparation and Dox incorporation. The drug was loaded at polymer-to-drug mass ratios of 10:1 and 10:3. The dialysis method produced the best results at a polymer-to-drug mass ratio 10:3 in terms of drug loading (DL 13.5 %) and encapsulation efficiency (EE 59 %) compared to the nanoprecipitation (DL 5 % and EE 54 %, at a polymer: drug mass ratio 10:1). Nevertheless, NanoStar@Dox obtained by dialysis had an average hydrodynamic diameter of > 500 nm and poor stability in aqueous solution; therefore, it was not advanced in the biological investigation. Conversely, nanoprecipitation enabled the production of NanoStar@Dox suitable for biological assays with a hydrodynamic diameter of approximately 278 nm, a monomodal particle size distribution, and a zeta potential value of −27 mV. Empty NanoStar with a particle size of approximately 251 nm were also prepared (Fig. S2).

The *core–shell* structure of NanoStar@Dox and drug incorporation were confirmed by NMR spectroscopy (Fig. 2). When NanoStar@Dox was solubilized in deuterium oxide D_2O (Fig. 2, red line), only the characteristic peak of PEG at 3.7 ppm was clearly visible, as expected, since amphiphilic copolymers self-assembled in water exposing the hydrophilic PEG moiety to the aqueous solution, while PLA moieties were not exposed to the water and the related NMR signals disappeared. The loss of crucial proton signals in D_2O confirmed that the water-soluble PEG constituted the outer shell of NanoStar@Dox and that the drug was readily incorporated into the polymeric nanocarrier. Conversely, the organic solvent dimethyl sulfoxide (DMSO-d_6) typically promoted the micellar disassembly, thereby all the peaks of PEG (3.5 ppm), PLA (5.2 and 1.5 ppm, main peaks) and Dox (small peaks between 8 and 1 ppm) were detected (Fig. 2, black line), according to literature (Oliva et al., 2023; Fazio et al., 2015).

3.3. RGD-NanoStar formulation and characterization

Nanoprecipitation was selected as the best nanoformulation method for RGD-NanoStar@Dox preparation and only the 10:3 polymer-to-drug mass ratio was investigated. A binary blend of *star* PLA-PEG-RGD and its precursor *star* PLA-PEG (1:9 mass ratio) was employed, according to literature reporting similar use of blended mixtures based on RGD-decorated and undecorated polyesters for NPs formation (Li et al., 2016; Diou et al., 2014). Briefly, an organic solution of the blended polymers and Dox HCl (in the presence of triethylamine for deprotonation) was added dropwise into an aqueous solution under stirring; dur-

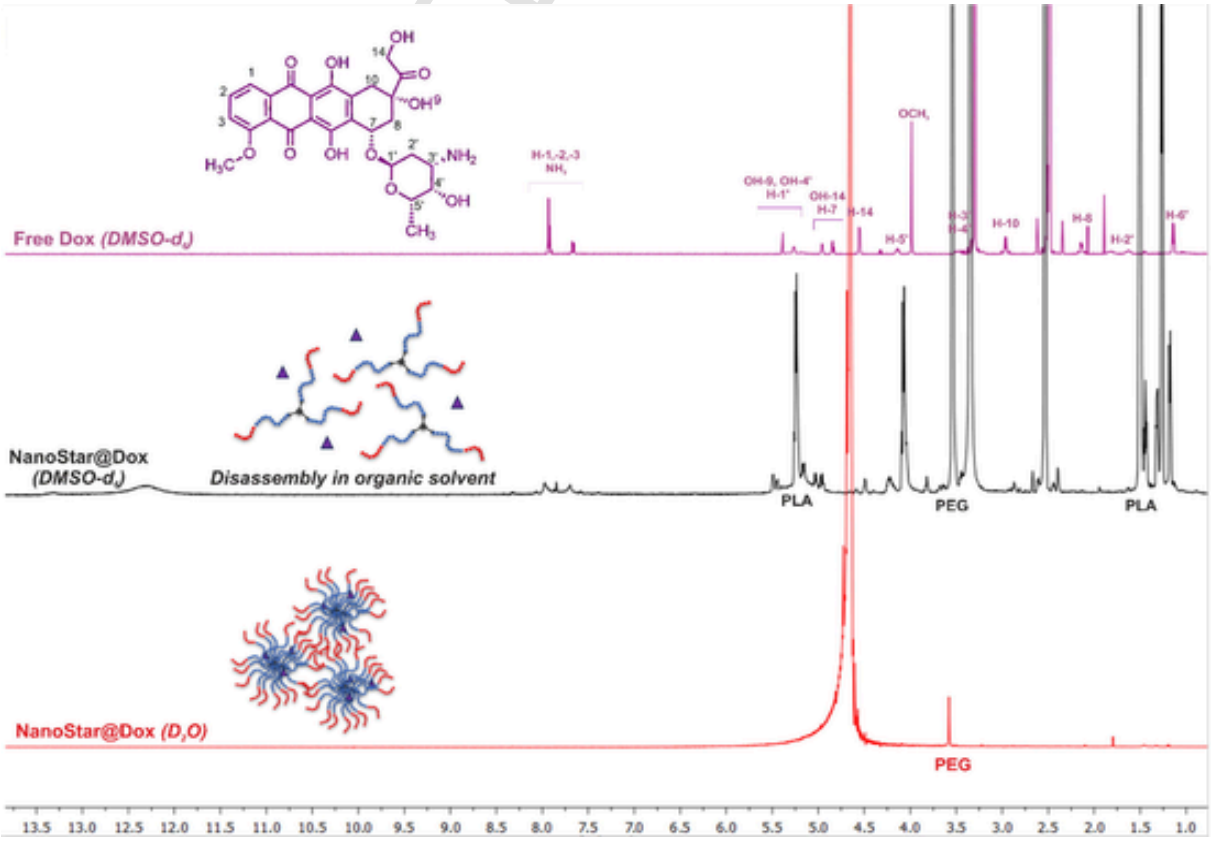

Fig. 2. Stacked ^{1}H NMR spectra of free Dox in DMSO-d_6 (violet), NanoStar@Dox in DMSO-d_6 (black) and NanoStar@Dox in D_2O (red). ^{1}H NMR spectrum of free Dox in DMSO-d_6 is reported for comparison with full proton assignment (Piorecka et al., 2017).

ing the rapid diffusion of the organic solution in the non-solvent, RGD-NanoStar@Dox were formed with a favorable drug loading (*i.e.,* 8 % DL; 35 % EE). DLS analysis showed a hydrodynamic diameter of about 349 nm for the main population (≅90 %) with a second negligible population (≅10 %) of about 80 nm and a ς-potential value of about −29 mV attesting for a good colloidal stability typical for aliphatic polyester NPs (Torcasio et al., 2022). Empty RGD-NanoStar were also obtained by nanoprecipitation with a smaller mean diameter (*i.e.,* about 259 nm for the main population ≅ 93 %; about 55 nm for the second negligible population ≅ 7 %) and a ς-potential value of about −20 mV (Fig. S2).

Negative zeta potential values are rather common for aliphatic polyester NPs attesting for good colloidal stability, reduced plasma protein bioadhesion and low rate of non-specific cellular uptake, being an advantage from a biopharmaceutical point of view (Zhang et al., 2012). This negative surface charge could be ascribed to a preferential adsorption/binding of negatively charged hydroxyl anions originated by water's autodissociation to the PEG chains of the *star* polymer at the interface between the PEGylated NPs and the aqueous solution, as suggested by the works of Johnsson (Johnsson et al., 2003) and Kreuzer (Kreuzer et al., 2003).

Particle size and morphology of RGD-NanoStar with and without drug were investigated by SEM analysis (Fig. 3). Empty RGD-NanoStar (Fig. 3A-B) seemed to have near-spherical shape with rough surface and size ranging from about 30 nm to 230 nm, the latter being assemblies of the smaller ones, as evident in Fig. 3B which provided the actual individual particle size. Moreover, the majority of the particles had diameters < 100 nm (Fig. 3A) which was in accordance with the polymer MW. The size values determined by DLS were, in average, higher compared to what SEM reported, as expected (Rahmani et al., 2021), since DLS measured the hydrodynamic diameter (or mean size) of our micellar nanoassemblies. This peculiar feature of DLS measurement was undoubtedly ascribed to the role of water or aqueous medium which hydrated the dispersed nanoassemblies leading to larger particle sizes, influencing their hydrodynamic properties and decreasing their diffusion coefficient. Conversely, in the dry condition of SEM analysis, the role of water in the NPs hydration was minimal due to its removal under vacuum before the measurement.

SEM data of RGD-NanoStar@Dox (Fig. 3C-F) revealed that the drug-loaded sample mainly consisted in particles with a diameter between about 50 and 220 nm and a rough surface. The particles morphology changed after drug loading which likely drove the formation of differently shaped nanoassemblies. A greater tendency to form larger assem-

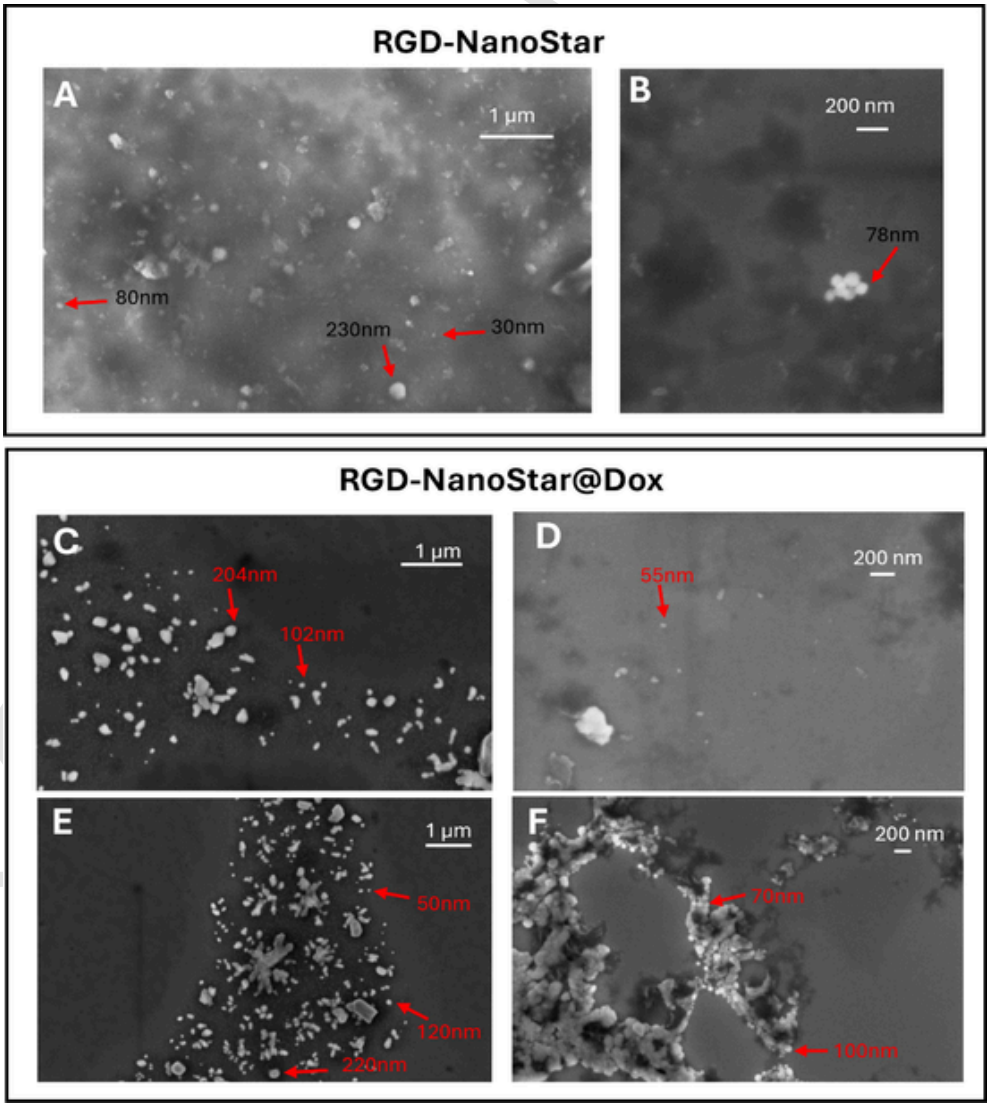

Fig. 3. SEM analysis of empty RGD-NanoStar (A-B) and RGD-NanoStar@Dox (C-F).

blies (multi-micellar aggregates) was observed for such sample with respect to the empty particles, as shown in Fig. 3D-E-F. It is well known that amphiphilic star polymers, due to the unique covalently reinforced *core–shell* structure, could exist as unimolecular micelles below their CMC and further self-assemble into multi-micellar aggregates at high concentration (Jin et al., 2018). Specifically, above the CMC, the unimolecular micelles undergo secondary aggregation to form multimolecular micelles due to the interactions between their arms. During the self-assembly, the interchain overlapping, entangling, and crumpling of the arms occurs, resulting in the accumulation of unimolecular micelles to multi-micellar aggregates (MMM mechanism) as well described by Karmegam and coworkers for their *star*-like polycaprolactone micelles loaded with Dox (Karmegam et al., 2021). It is worth noting that the formation of multi-micellar aggregates from unimolecular micelles is a dynamic and gradual process, thus the coexistence of these two different micelles can be sometimes observed. However, for majority of *star* polymers, it is difficult to direct visualize the defined core and isolated arms, but only near-spherical particles can be observed (Jin et al., 2018) missing the fine structural details of these architecturally complex macromolecules (Ren et al., 2016).

The drug release profile of RGD-NanoStar@Dox was investigated under physiologically relevant conditions (PBS, pH 7.4; Fig. 4A) and compared with the release behavior of both untargeted NanoStar@Dox and free drug. Wavelengths of 500 and 480 nm were the characteristic absorption peaks of loaded and free Dox, respectively, in PBS (Fig. S3), with the typical red-shift being the result of Dox encapsulation into the nanocarrier, according to literature (Zhang et al., 2023).

Under our experimental conditions, NanoStar@Dox did not release the incorporated drug within 72 h, whereas free Dox had a very quick release, as expected, due to the rapid diffusion across the dialysis membrane, reaching approximately 41 % in the first 45 min, 70 % in 5 h, and 73 % in 8 h (inset Fig. 4A; Table S1).

Conversely, RGD-NanoStar@Dox released the drug in a more sustained and prolonged manner with respect to free Dox reaching approximately 17 % within the initial 24 h (Fig. 4A; Table S1). Specifically, only about 3 % of Dox was released from RGD-NanoStar@Dox in the first 45 min, likely ascribed to the drug molecules loosely held to or embedded near the NPs surface, reaching 12 % at 5 h and 15 % at 8 h. Overall, a gradual and sustained release of the drug was obtained over 72 h.

Since we experienced that the drug release was affected by Dox precipitation over the time, we would like to point out that the knowledge of this phenomenon is strictly necessary for a correct data interpretation.

Despite numerous papers investigated, so far, the incorporation of Dox into polymeric NPs and their related anticancer efficacy, few attempts have considered evaluating the dimerization and consequent precipitation of Dox occurring under physiologically relevant conditions (Yamada 2020; Dornjak et al., 2022; Kovshova et al., 2021). The topic was recently well investigated by Yamada (Yamada 2020) which proposed a mechanism for Dox dimerization in buffer involving the α-hydroxy ketone and a structure for the Dox dimer based on mass spectrometry in combination with a reaction model with hydroxylamine in PBS.

Based on these findings, we investigated Dox stability in phosphate buffer (pH 7.4) at 37 °C by monitoring the UV–Vis absorption of a reference solution at three different concentrations over 72 h: the concentration of Dox rapidly decreased in the supernatant (Fig. 4B and Fig. S4) and Dox precipitation (see photograph in Fig. 4B) resulted ~ 10 % after 6 h and 24 %, 50 %, 65 % after 24 h, 48 h, and 72 h, respectively (Table S1), regardless of the initial drug concentration.

Our findings pointed out that a prolonged exposure of Dox in aqueous solution during the release experiments may generate inaccurate results in terms of cumulative percentage release owing to Dox dimer formation and precipitation. Indeed, in our release experiment of free Dox, we detected at late time points (*i.e.,* 24–72 h) a percentage of Dox released in the receiving compartment lower than the previous time points (Table S1). Therefore, the percentage of Dox that underwent dimerization and precipitation should be considered for a proper interpretation of release data. Specifically, although at earlier time points the precipitation of Dox dimer did not strongly influence the release profile (8 % of Dox dimer formation within 5 h), at later time points (> 6h), free Dox concentration rapidly decreased (50 % of Dox dimer formation after 48 h) and strongly affected the release data. Therefore, the ratio between drug release and drug degradation is responsible for the detected concentration in the receiver compartment.

Altogether, the findings of the present and previous studies suggest that Dox chemical transformation producing Schiff base linkages needs to be considered and further investigated since dimerization seemed to alter the intracellular localization of Dox (Yamada 2020, Fukushima et al., 1999; Yokoyama et al., 1998) and the reaction involving the reactive α-hydroxy ketone can occur not only between two Dox molecules but also between Dox and other bio-relevant compounds containing amine groups (*e.g.,* serum proteins) (Zunino et al., 1981) influencing pharmacokinetics and pharmacological effects *in vivo* and *in vitro*.

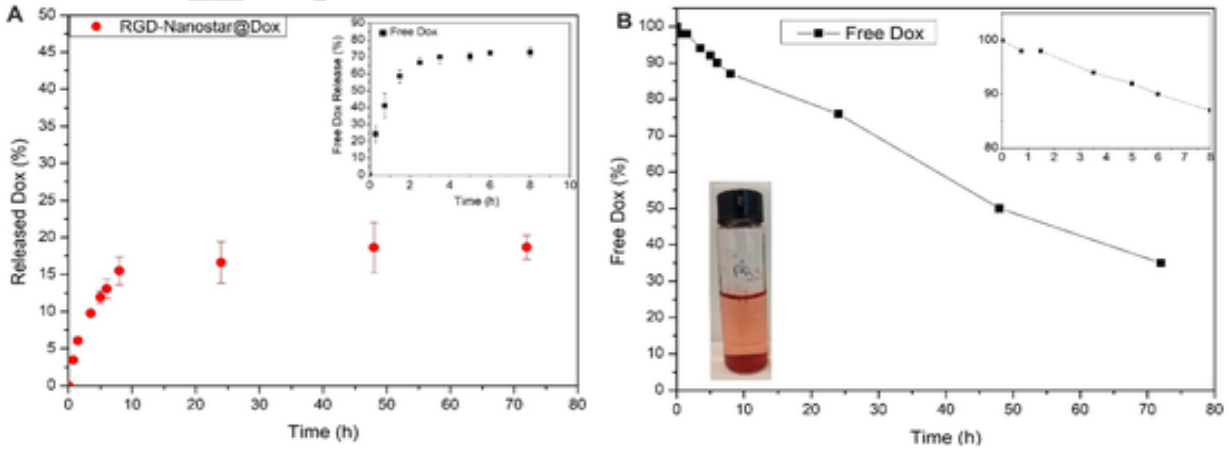

Fig. 4. (A) Release profile of Dox from RGD-NanoStar@Dox (●) in PBS at 37 °C; inset: release of free Dox (■) under the same experimental conditions. Data are shown as mean ± SD (n = 2). (B) Free Dox stability study with related photograph. Reference solution of free Dox in PBS at 37 °C underwent dimerization and precipitation leading to a decrease of drug concentration in the supernatant monitored by UV–Vis. Inset shows a zoomed-in version of the data for the first 8 h.

In summary, our stability and release experiments revealed the crucial role of RGD-NanoStar as protective sleeves for Dox. Release experiments attested that RGD-NanoStar@Dox was able to supply about 20 % of active monomeric Dox within 72 h; the remain undetected portion (about 80 %) can be considered as a Dox *"reservoir"*, although it could be partially affected by Dox degradation over the time. Since our stability study attested a dimeric Dox formation ranging from 2 to 65 % within 72 h (Table S1), we can estimate a *"reservoir"* pool of drug of about 78–15 % still available in RGD-NanoStar micellar nanoassemblies to be released after 72 h.

3.4. Biology

To determine the anticancer effect of both the proposed systems, with and without RGD-tagging, the behavior of different osteosarcoma cell lines (*i.e.,* MG63, SAOS-2, and U2-OS) and healthy osteoblast cells (hFOBs) grown for 72 h in the presence of loaded and unloaded micellar nanoassemblies was biologically characterized.

The cellular uptake experiment, evaluated by the detection of fluorescent Dox localization, demonstrated that Dox loaded on RGD-NanoStar easily reached the cell nuclei at 72 h, as well as free Dox, as confirmed by the colocalization with the DAPI fluorescence signal (Fig. 5). Surprisingly, untargeted NanoStar@Dox showed cytoplasmic localization indicating that the drug internalized by NanoStar did not reach the cell nuclei (Fig. 5), in line with the outcome of the release experiment.

The viability of all cell lines treated with NanoStar@Dox (5.4 μg/mL drug concentration) was assessed by MTT assay to confirm the uptake, resulting in absent or extremely low cytotoxic activity compared to free Dox (Fig. S5).

It is well known that free Dox rapidly diffuses into the nucleus and the inhibition of topoisomerase-II has been referred as one of the major cytotoxic effects (Mitry and Edwards, 2016). Usually, Dox is released from nanosystems upon their lysosomal processing reaching the nucleus very fast within 24–48 h (Nandi et al., 2020). Our results demonstrated that NanoStar@Dox was concentrated in the cytoplasm, probably inside the lysosomes as the principal intracellular location of NPs. However, the typical acidic and enzymatic lysosomal digestion did not guarantee the drug release from NanoStar@Dox and, accordingly, no cytotoxic effect was observed under our experimental conditions.

Conversely, the contribution of the peptidic RGD moiety resulted crucial in terms of biological effects for RGD-tagged micellar nanoassemblies: in fact, RGD-NanoStar@Dox produced the same cytotoxic effect as free Dox in all the cell lines and at all the tested concentrations (Fig. 6), in line with the observed nuclear localization (Fig. 5).

Notably, the antitumor activity of Dox released from RGD-NanoStar@Dox was well preserved and our nanosystem served as a *"drug reservoir"* providing sustained Dox release. Moreover, we would like to point out that the biological effects observed in MTT assay after 72 h of treatment (Fig. 6) should be considered taking into account the outcomes of our release experiments (*e.g.,* only about 19 % of the loaded drug was detected in its "native" and active form in the receiver compartment after 72 h). Therefore, one of the main advantages of the proposed nanosystem is the protection of the drug from dimerization under physiologically relevant conditions and, consequently, an extended biological activity over the time.

Focusing on the biological effect of unloaded RGD-NanoStar, our results demonstrated a total absence of cytotoxicity in healthy osteoblasts (hFOBs; Fig. 6A) and various cytotoxic effects in cancer cells (Fig. 6B-D) likely due to their intrinsic biological differences (*i.e.,* expression of $\alpha_v\beta_3$ and $\alpha_v\beta_5$ integrins) (Visvader 2011; Fang et al., 2017). Specifically,

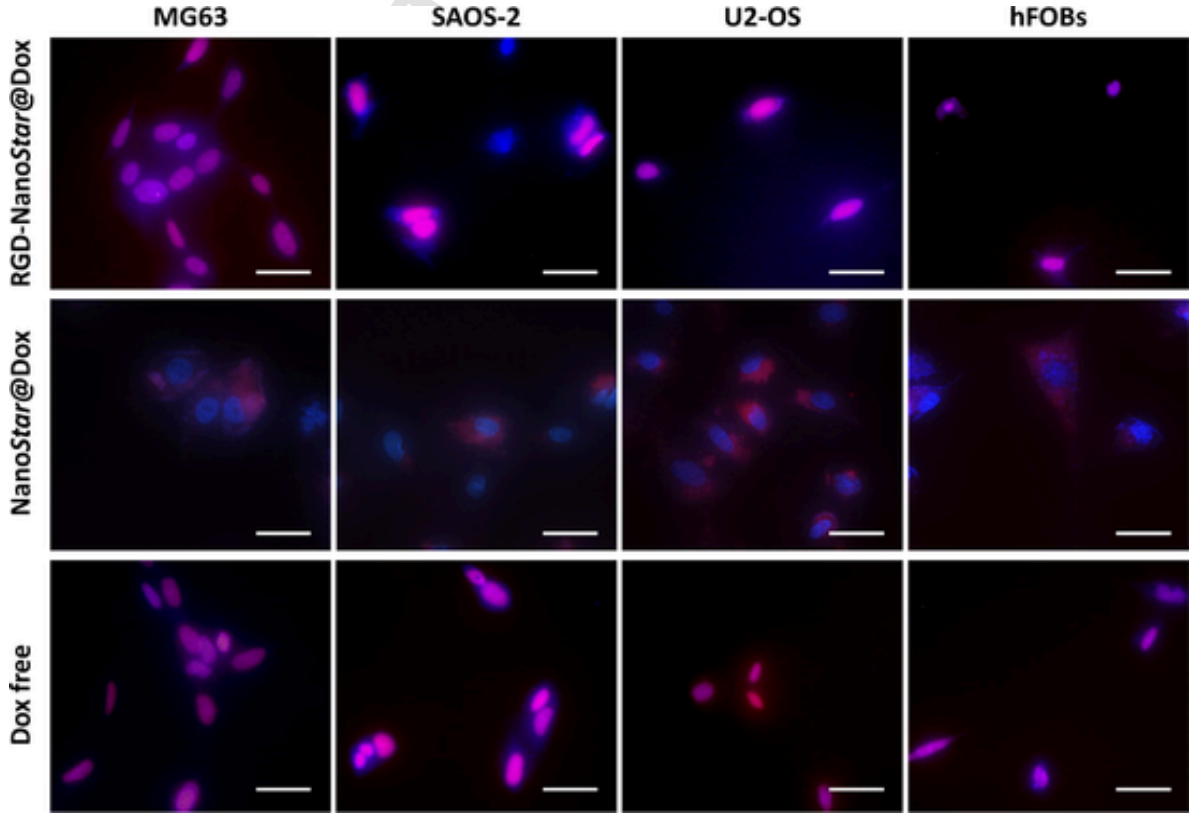

Fig. 5. Cellular uptake. The internalization of RGD-NanoStar@Dox in cell nuclei compared to NanoStar@Dox and free Dox was reported for 5.4 μg/mL drug concentration in all the cell lines. Cell nuclei in blue (DAPI), internalized Dox in purple (DAPI + TRITC). Scale bars 50 μm.

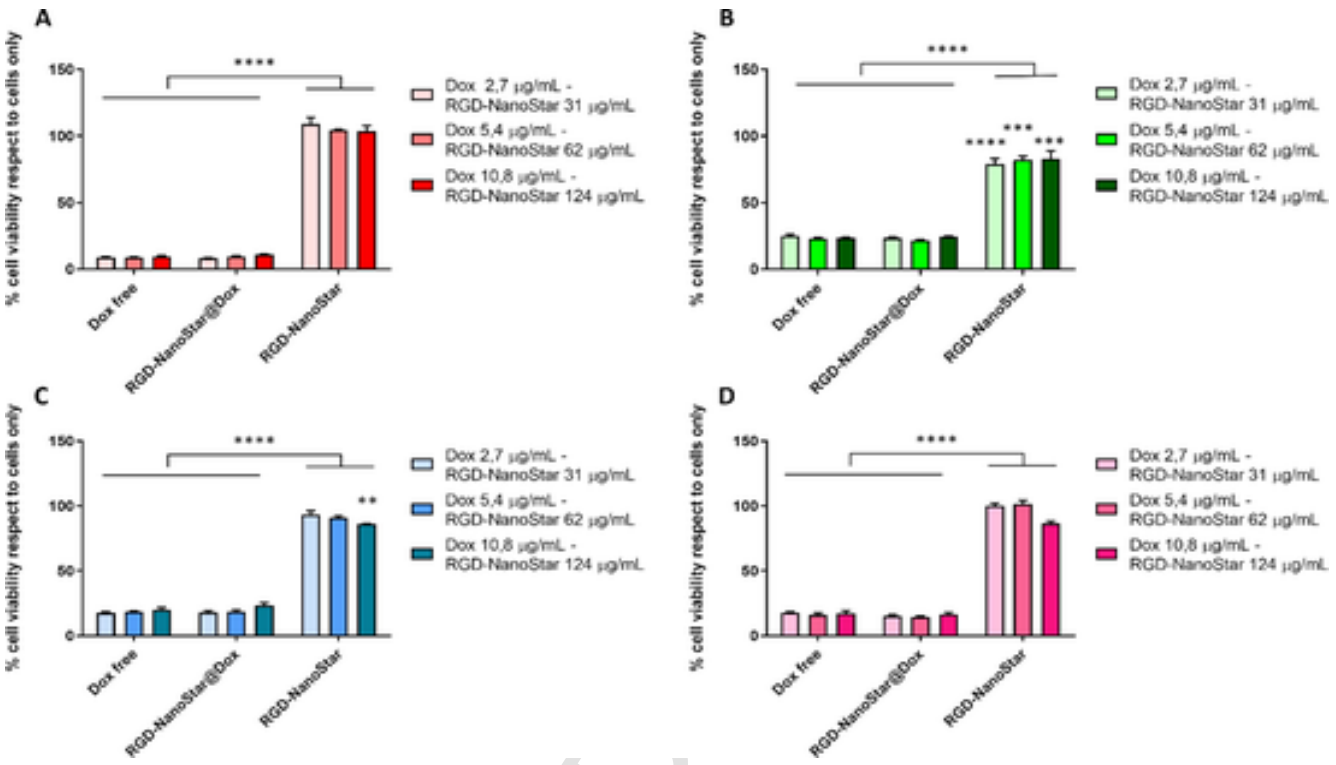

Fig. 6. MTT assay. Cell viability evaluation of hFOBs (A), MG63 (B), SAOS-2 (C) and U2-OS (D) after 72 h of culture with RGD-NanoStar@Dox, unloaded RGD-NanoStar and free Dox. The graphs show the % of cell viability with respect to cells only (mean ± standard error of the mean). ** p value ≤ 0.01, *** p value ≤ 0.001, **** p value ≤ 0.0001.

empty RGD-NanoStar statistically significantly reduced the viability of MG63 at all the tested concentrations and with a dose-dependent trend in SAOS-2 compared to cells only (Fig. 6B and 6C), but it seemed do not compromise the viability of U2-OS even at the highest tested concentration (Fig. 5D).

Furthermore, morphological analysis of the cells treated with RGD-NanoStar confirmed the observed results underlining that, even if present, the cytotoxicity of our micellar nanoassemblies was limited and the surviving cells maintained their typical morphology without evident nuclear or cytokinetic damage (Fig. 7).

4. Conclusion

In summary, this work describes the preparation of biocompatible polymeric micellar nanoassemblies based on three-armed *star* PLA-PEG and *star* PLA-PEG-RGD copolymers loaded with Doxorubicin as anticancer nanotherapeutics for osteosarcoma treatment. Optimized nanoparticles were prepared by nanoprecipitation of *star* PLA-PEG block copolymers (untargeted NanoStar) or blends of *star* PLA-PEG and *star* PLA-PEG-RGD (targeted RGD-NanoStar). Typical *core–shell* nanostructures were obtained with a satisfactory Dox payload (8 % drug loading for RGD-NanoStar@Dox; 5 % drug loading for NanoStar@Dox). Controlled and sustained drug release behavior was observed for RGD-NanoStar@Dox with a release rate significantly lower than that of the free drug under the same concentration and experimental conditions, whereas no drug release was detected for NanoStar@Dox. In line with these results, *in vitro* biological studies demonstrated the failure of NanoStar@Dox to reach the nucleus and consequent ineffectiveness against osteosarcoma cells; conversely, the ability of RGD-NanoStar@Dox to deliver Dox into the nucleus of MG63, SAOS-2, and U2-OS cells led to significant cytotoxic effects without compromising the viability of healthy osteoblasts. Overall, cell studies confirmed the cytocompatibility of our nanosystems and their effective antitumoral properties, highlighting the pivotal role of cyclic RGD peptide in driving cellular uptake and accumulation in osteosarcoma cells. RGD-integrin recognition enables polymeric micelles to actively target tumor cells and enhances endocytosis; as a result, greater cellular uptake and intracellular release of the drug were achieved with RGD-

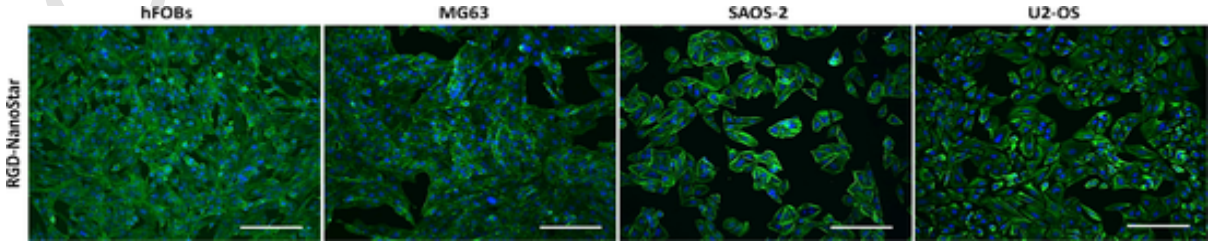

Fig. 7. Morphological analysis. Cell morphology evaluation of all cell lines in the presence of unloaded RGD-NanoStar (124 μg/mL). Cell nuclei in blue, F-actin filaments in green. Scale bars 200 μm.

NanoStar@Dox respect to undecorated micellar nanoassemblies. Targeting drugs to their sites of action remains a major challenge in pharmaceutical research to overcome systemic side effects associated with most antineoplastic agents. Future studies will investigate the behavior of these *star*-shaped micellar nanoassemblies *in vivo*.

CRediT authorship contribution statement

Roberto Oliva: Investigation, Formal analysis. **Serena Maria Torcasio:** Investigation, Formal analysis. **Olivier Coulembier:** Validation, Methodology. **Anna Piperno:** Writing – review & editing, Validation, Methodology. **Antonino Mazzaglia:** Investigation, Formal analysis. **Silvia Scalese:** Writing – review & editing, Data curation. **Arianna Rossi:** Investigation, Formal analysis. **Giada Bassi:** Investigation, Formal analysis. **Silvia Panseri:** Writing – review & editing, Data curation. **Monica Montesi:** Writing – review & editing, Writing – original draft, Supervision, Data curation. **Angela Scala:** Writing – review & editing, Writing – original draft, Supervision, Investigation, Funding acquisition, Data curation, Conceptualization.

Declaration of competing interest

The authors declare that they have no known competing financial interests or personal relationships that could have appeared to influence the work reported in this paper.

Data availability

Data will be made available on request.

Acknowledgments

This work was partially supported by the European Union – Next Generation EU - Projects PRIN 2022 (2022P99NY5) “FINE” (CUP Master J53D23008760006) and PRIN 2022 PNRR (P202242X25) “MERCURY” (CUP Master B53D23031930001). O.C. is Senior Research for F.R.S.-FNRS and an AXA Professor in Chemistry at UMons.

Appendix A. Supplementary data

Supplementary data to this article can be found online at https://doi.org/10.1016/j.ijpharm.2024.124183.

References

Agrahari, V., Agrahari, V., 2018. Advances and applications of block-copolymer-based nanoformulations. Drug Discov. Today. 23, 1139–1151. https://doi.org/10.1016/j.drudis.2018.03.004.

Battistini, L., Bugatti, K., Sartori, A., Curti, C., Zanardi, F., 2021. RGD peptide-drug conjugates as effective dual targeting platforms: recent advances. Eur. J. Org. Chem. 17, 2506–2528. https://doi.org/10.1002/ejoc.202100240.

Diou, O., Fattal, E., Delplace, V., Mackiewicz, N., Nicolas, J., Mériaux, S., Valette, J., Robic, C., Tsapis, N., 2014. RGD decoration of PEGylated polyester nanocapsules of perfluorooctyl bromide for tumor imaging: Influence of pre or post-functionalization on capsule morphology. Eur. J. Pharm. Biopharm. 87, 170–177. https://doi.org/10.1016/j.ejpb.2013.12.003.

Dornjak, L., Kovačić, M., Ostojić, K., Angaits, A., Szpunar, J., Urlić, I., Rogina, A., 2022. Chitosan-boric acid scaffolds for doxorubicin delivery in the osteosarcoma treatment. Polymers 14, 4753. https://doi.org/10.3390/polym14214753.

Fang, Z., Sun, Y., Xiao, H., Li, P., Liu, M., Ding, F., Kan, W., Miao, R., 2017. Targeted osteosarcoma chemotherapy using RGD peptide-installed doxorubicin-loaded biodegradable polymeric micelle. Biomed. Pharmacother. 85, 160–168. https://doi.org/10.1016/j.biopha.2016.11.132.

Fazio, E., Scala, A., Grimato, S., Ridolfo, A., Grassi, G., Neri, F., 2015. Laser light triggered smart release of silibinin from a PEGylated–PLGA gold nanocomposite. J. Mater. Chem. B. 3, 9023–9032. https://doi.org/10.1039/C5TB01076D.

Fukushima, S., Machida, M., Akutsu, T., Shimizu, K., Tanaka, S., Okamoto, K., Mashiba, H., Yokoyama, M., Okano, T., Sakurai, Y., Kataoka, K., 1999. Roles of adriamycin and adriamycin dimer in antitumor activity of the polymeric micelle carrier system. Colloids Surf. B. 16, 227–236. https://doi.org/10.1016/S0927-7765(99)00073-9.

Gianferante, D.W., Mirabello, L., Savage, S.A., 2017. Germline and somatic genetics of osteosarcoma - connecting aetiology, biology and therapy. Nat. Rev. Endocrinol. 13, 480–491. https://doi.org/10.1038/nrendo.2017.16.

Govender, T., Riley, T., Ehtezazi, T., Garnett, M.C., Stolnik, S., Illum, L., Davis, S.S., 2000. Defining the drug incorporation properties of PLA–PEG Nanoparticles. Int. J Pharm. 199, 95–110. https://doi.org/10.1016/S0378-5173(00)00375-6.

Jin, X., Sun, P., Tong, G., Zhu, X., 2018. Star polymer-based unimolecular micelles and their application in bio-imaging and diagnosis. Biomaterials 178, 738–750. https://doi.org/10.1016/j.biomaterials.2018.01.051.

Johnsson, M., Wagenaar, A., Engberts, J.B.F.N., 2003. Sugar-based gemini surfactant with a vesicle-to-micelle transition at acidic pH and a reversible vesicle flocculation near neutral pH. J. Am. Chem. Soc. 125, 757–760. https://doi.org/10.1021/ja028195t.

Karmegam, V., Kuruppu, S.S., Gedara, C.M.U., Biewer, M.C., Stefan, M.C., 2021. Enhanced DOX loading in star-like benzyl functionalized polycaprolactone micelles. J. Polym. Sci. 59, 3040–3052. https://doi.org/10.1002/pol.20210544.

Kovshova, T., Osipova, N., Alekseeva, A., Malinovskaya, J., Belov, A., Budko, A., Pavlova, G., Maksimenko, O., Nagpal, S., Braner, S., Modh, H., Balabanyan, V., Wacker, M.G., Gelperina, S., 2021. Exploring the interplay between drug release and targeting of lipid-like polymer nanoparticles loaded with doxorubicin. Molecules 26, 831. https://doi.org/10.3390/molecules26040831.

Kreuzer, H.J., Wang, R.L.C., Grunze, M., 2003. Hydroxide ion adsorption on self-assembled monolayers. J. Am. Chem. Soc. 125, 8384–8389. https://doi.org/10.1021/ja0350839.

Kuperkar, K., Patel, D., Atanase, L.I., Bahadur, P., 2022. Amphiphilic block copolymers: their structures, and self-assembly to polymeric micelles and polymersomes as drug delivery vehicles. Polymers 14, 4702. https://doi.org/10.3390/polym14214702.

Li, N., Qiu, S., Fang, Y., Wu, J., Li, Q., 2021. Comparison of linear vs. cyclic RGD pentapeptide interactions with integrin αvβ3 by molecular dynamics simulations. Biology (Basel) 10, 688. https://doi.org/10.3390/biology10070688.

Li, C., Wanga, W., Xi, Y., Wang, J., Chen, J.-F., Yun, J., Le, Y., 2016. Design, preparation and characterization of cyclic RGDfK peptide modified poly(ethylene glycol)-blockpoly(lactic acid) micelle for targeted delivery. Mater. Sci. Eng. C. 64, 303–309. https://doi.org/10.1016/j.msec.2016.03.062.

Liénard, R., Montesi, M., Panseri, S., Dozio, S.M., Vento, F., Mineo, P.G., Piperno, A., De Winter, J., Coulembier, O., Scala, A., 2020. Design of naturally inspired jellyfish-shaped cyclo-polylactides to manage osteosarcoma cancer stem cells fate. Mater. Sci. Eng. C. 117, 111291. https://doi.org/10.1016/j.msec.2020.111291.

Liu, J., Lin, S., Dang, J., Wang, S., Cheng, W., Ran, Z., Zhu, H., Deng, H., Xiong, C., Xu, W., Huang, Z., Xu, P., Xu, H., 2023. Anticancer and bone-enhanced nano-hydroxyapatite/gelatin/polylactic acid fibrous membrane with dual drug delivery and sequential release for osteosarcoma. Int. J. Biol. Macromol. 240, 124406. https://doi.org/10.1016/j.ijbiomac.2023.124406.

Lotocki, V., Kakkar, A., 2020. Miktoarm star polymers: branched architectures in drug delivery. Pharmaceutics. 12, 827. https://doi.org/10.3390/pharmaceutics12090827.

Lupusoru, R., Pricop, D.A., Uritu, C.M., Arvinte, A., Coroaba, A., Esanu, I., Zaltariov, M.F., Silion, M., Stefanescu, C., Pinteala, M., 2020. Effect of TAT-DOX-PEG irradiated gold nanoparticles conjugates on human osteosarcoma cells. Sci. Rep. 10, 6591. https://doi.org/10.1038/s41598-020-63245-8.

Mineo, P.G., Foti, C., Vento, F., Montesi, M., Panseri, S., Piperno, A., Scala, A., 2020. Salinomycin-loaded PLA nanoparticles: drug quantification by GPC and wave voltammetry and biological studies on osteosarcoma cancer stem cells. Anal. Bioanal. Chem. 412, 4681–4690. https://doi.org/10.1007/s00216-020-02721-6.

Mitry, M.A., Edwards, J.G., 2016. Doxorubicin induced heart failure: Phenotype and molecular mechanisms. Int. J. Cardiol. Heart Vasc. 10, 17–24. https://doi.org/10.1016/j.ijcha.2015.11.004.

Nandi, S., Kale, N., Patil, A., Banerjee, S., Patil, Y., Khandare, J., 2020. A graphene-sandwiched DNA nano-system: regulation of intercalated doxorubicin for cellular localization. Nanoscale Adv. 2, 5746–5759. https://doi.org/10.1039/D0NA00575D.

Oliva, R., Ginestra, G., Piperno, A., Mazzaglia, A., Nostro, A., Scala, A., 2023. Harnessing the power of PLA-PEG nanoparticles for linezolid delivery against methicillin-resistant *Staphylococcus aureus*. Int. J. Pharm. 642, 123067. https://doi.org/10.1016/j.ijpharm.2023.123067.

Panez-Toro, I., Muñoz-García, J., Vargas-Franco, J.W., Renodon-Cornière, A., Heymann, M.-F., Lézot, F., Heymann, D., 2023. Advances in osteosarcoma. Curr. Osteoporos. Rep. 21, 330–343. https://doi.org/10.1007/s11914-023-00803-9.

Parchami, M., Haghiralsadat, F., Sadeghian-Nodoushan, F., Hemati, M., Shahmohammadi, S., Ghasemi, N., Sargazi, G., 2023. A new approach to the development and assessment of doxorubicin-loaded nanoliposomes for the treatment of osteosarcoma in 2D and 3D cell culture systems. Heliyon. 9, e15495.

Piorecka, K., Stanczyk, W., Florczak, M., 2017. NMR analysis of antitumor drugs: Doxorubicin, daunorubicin and their functionalized derivatives. Tetrahedron Lett. 58, 152–155. https://doi.org/10.1016/j.tetlet.2016.11.118.

Piperno, A., Sciortino, M.T., Giusto, E., Montesi, M., Panseri, S., Scala, A., 2021. Recent advances and challenges in gene delivery mediated by polyester-based nanoparticles. Int. J. Nanomed. 16, 5981–6002. https://doi.org/10.2147/IJN.S321329.

Rahmani, A., Rahimi, F., Iranshahi, M., Kahroba, H., Zarebkohan, A., Talebi, M., Salehi, R., Mousavi, H.Z., 2021. Co-delivery of doxorubicin and conferone by novel pH-responsive β-cyclodextrin grafted micelles triggers apoptosis of metastatic human breast cancer cells. Sci. Rep. 11, 21425. https://doi.org/10.1038/s41598-021-00954-8.

Ren, J.M., McKenzie, T.G., Fu, Q., Wong, E.H.H., Xu, J., An, Z., Shanmugam, S., Davis, T.P., Boyer, C., Qiao, G.G., 2016. Star polymers. Chem Rev. 116, 6743–6836. https://doi.org/10.1021/acs.chemrev.6b00008.

Riley, T., Stolnik, S., Heald, C.R., Xiong, C.D., Garnett, M.C., Illum, L., Davis, S.S., 2001. Physicochemical evaluation of nanoparticles assembled from poly(lactic acid)-poly (ethylene glycol) (PLA-PEG) block copolymers as drug delivery vehicles. Langmuir 17, 3168–3174. https://doi.org/10.1021/la001226i.

Rios De La Rosa, J.M., Spadea, A., Donno, R., Lallana, E., Lu, Y., Puri, S., Caswell, P.,

Lawrence, M.J., Ashford, M., Tirelli, N., 2020. Microfluidic-assisted preparation of RGD-decorated nanoparticles: exploring integrin-facilitated uptake in cancer cell lines. Sci. Rep. 10, 14505. https://doi.org/10.1038/s41598-020-71396-x.

Scala, A., Piperno, A., Micale, N., Mineo, P.G., Abbadessa, A., Risoluti, R., Castelli, G., Bruno, F., Vitale, F., Cascio, A., Grassi, G., 2018. "Click" on PLGA-PEG and hyaluronic acid: Gaining access to anti-leishmanial pentamidine bioconjugates. J. Biomed. Mater. Res. B Appl. Biomater. 106, 2778–2785. https://doi.org/10.1002/jbm.b.34058.

Song, X., Yan, T., Tian, F., Li, F., Ren, L., Li, Q., Zhang, S., 2021. Aptamer functionalized upconversion nanotheranostic agent with nuclear targeting as the highly localized drug-delivery system of doxorubicin. Front. Bioeng. Biotechnol. 9, 639487. https://doi.org/10.3389/fbioe.2021.639487.

Sun, Y., Kang, C., Liu, F., Zhou, Y., Luo, L., Qiao, H., 2017. RGD peptide-based target drug delivery of doxorubicin nanomedicine. Drug Dev. Res. 78, 283–291. https://doi.org/10.1002/ddr.21399.

Torcasio, S.M., Oliva, R., Montesi, M., Panseri, S., Bassi, G., Mazzaglia, A., Piperno, A., Coulembier, O., Scala, A., 2022. Three-armed RGD-decorated starPLA-PEG nanoshuttle for docetaxel delivery. Biomater. Adv. 140, 213043. https://doi.org/10.1016/j.bioadv.2022.213043.

Visvader, J.E., 2011. Cells of origin in cancer. Nature 469, 314–322. https://doi.org/10.1038/nature09781.

Wang, S.-Y., Hu, H.-Z., Qing, X.-C., Zhang, Z.-C., Shao, Z.-W., 2020. Recent advances of drug delivery nanocarriers in osteosarcoma treatment. J. Cancer. 11, 69–82. https://doi.org/10.7150/jca.36588.

Wei, H., Chen, F., Chen, J., Lin, H., Wang, S., Wang, Y., Wu, C., Lin, J., Zhong, G., 2022. Mesenchymal stem cell derived exosomes as nanodrug carrier of doxorubicin for targeted osteosarcoma therapy via SDF1-CXCR4 axis. Int. J. Nanomed. 17, 3483–3495. https://doi.org/10.2147/IJN.S372851.

Yamada, Y., 2020. Dimerization of doxorubicin causes its precipitation. ACS Omega 5, 33235–33241. https://doi.org/10.1021/acsomega.0c04925.

Yang, P., Zhang, L., Wang, T., Liu, Q., Wang, J., Wang, Y., Tu, Z., Lin, F., 2020. Doxorubicin and edelfosine combo-loaded lipid-polymer hybrid nanoparticles for synergistic anticancer effect against drug-resistant osteosarcoma. Onco Targets Ther. 13, 8055–8067. https://doi.org/10.2147/OTT.S259428.

Yokoyama, M., Fukushima, S., Uehara, R., Okamoto, K., Kataoka, K., Sakurai, Y., Okano, T., 1998. Characterization of physical entrapment and chemical conjugation of adriamycin in polymeric micelles and their design for in vivo delivery to a solid tumor. J. Control. Release. 50, 79–92. https://doi.org/10.1016/S0168-3659(97)00115-6.

Zhang, L., Guo, Q., Zheng, R., Yu, Q., Liang, Y., Ma, G., Li, Q., Zhang, X., Xiao, H., Wang, L., 2023. Zwitterionic targeting doxorubicin-loaded micelles assembled by amphiphilic dendrimers with enhanced antitumor performance. Langmuir 39, 4766–47767. https://doi.org/10.1021/acs.langmuir.3c00159.

Zhang, C., Wang, W., Liu, T., Wu, Y., Guo, H., Wang, P., Tian, Q., Wang, Y., Yuan, Z., 2012. Doxorubicin-loaded glycyrrhetinic acid-modified alginate nanoparticles for liver tumor chemotherapy. Biomaterials 33, 2187e2196. https://doi.org/10.1016/j.biomaterials.2011.11.045.

Zunino, F., Gambetta, R.A., Zaccara, A., Carsana, R., 1981. A Differential interaction of doxorubicin and daunorubicin with human serum proteins. Tumori J. 67, 399–403. https://doi.org/10.1177/030089168106700502.